Atom Interferometer Measurement of the Newtonian Constant of Gravity

J. B. Fixler,[1] G. T. Foster,[2] J. M. McGuirk,[3] M. A. Kasevich[1]*

We measured the Newtonian constant of gravity, G, using a gravity gradiometer based on atom interferometry. The gradiometer measures the differential acceleration of two samples of laser-cooled Cs atoms. The change in gravitational field along one dimension is measured when a well-characterized Pb mass is displaced. Here, we report a value of $G = 6.693 \times 10^{-11}$ cubic meters per kilogram second squared, with a standard error of the mean of $\pm 0.027 \times 10^{-11}$ and a systematic error of $\pm 0.021 \times 10^{-11}$ cubic meters per kilogram second squared. The possibility that unknown systematic errors still exist in traditional measurements makes it important to measure G with independent methods.

The weak coupling of gravity compared with other forces makes precision gravity experiments difficult. This is manifested in the relatively poor knowledge of the Newtonian constant of gravity, G, compared with our understanding of other fundamental constants (*1*). The traditional torsion pendulum method for measuring G involves a well-characterized moving source mass that produces a torque on a test mass attached to a long fiber. Measurement of the test mass displacement, coupled with knowledge of the mechanics of the pendulum and of the source–test mass gravitational force, determines G. Other recent methods make use of a Fabry-Perot optical cavity (*2*), a flexure-strip balance (*3*), or a falling corner-cube gravimeter (*4*). The first direct precision measurement of G (*5*) determined the value of G to 1.1 parts per thousand (ppt), which remained the standard definition until 1942 (*6*), when the precision was increased to 0.45 ppt. During the past two decades, a number of high-precision measurements have been performed, but their discrepancies were larger than their standard deviations. Therefore, the accepted precision remained relatively unchanged (*7*, *8*). Recently, a few experiments have claimed to reach to <100 parts per million (ppm) (*9*–*11*).

The inherent difficulty of measuring G was evident in the change of the Committee on Data for Science and Technology (CODATA) definition from 1986 to 1998 (*1*, *8*), increasing the uncertainty to 1.5 ppt. Part of this increase came from an 83-ppm measurement in 1996 (*11*)—determined with the use of a dynamic fiberless torsion balance—that differed by 42 standard deviations from the CODATA value of G at the time. Questions were raised about the accuracy of other experiments as well. Also taken into account in the CODATA decision was a discovery of fiber twist anelasticity (*12*) in torsion balance experiments. Not until recently were the systematics of the experiment by Michaelis *et al.* (*11*) understood (*13*), resulting in the treatment of those results as outlier points.

We used quantum interference of atomic Cs to directly probe the gravitational scalar potential. The performance of instruments based on this technique meets or exceeds that of other state-of-the-art gravity (*14*) or gravity-gradient (*15*) devices. In this work, we used a gravity gradiometer to make a proof-of-principle measurement of G. We measured the differential acceleration of two laser-cooled ensembles of atomic Cs induced by a 540-kg Pb source mass precisely positioned between two vertically separated de Broglie wave gravimeters. With accurate knowledge of the atomic trajectories and the Pb source geometry and composition, we calculated the gravitationally induced phase shift in our atom interferometer and extracted a value for G. The accuracy was characterized with a thorough study of systematics that might influence our measurement. This method is loosely analogous to that of Schwarz *et al.* (*4*), who used macroscopic masses rather than interfering atomic wavepackets.

Our gravity gradiometer consists of two gravimeters that operate by the light-pulse atom interferometry technique (Fig. 1) (*16*). The momentum recoil from the emission or absorption of photons by a Cs atom is used to coherently split and deflect the atomic wavepackets. A $\pi/2$ "splitter" pulse places an atom initially in the ground state with momentum p into a superposition of ground and excited states, $|g,p\rangle \rightarrow (|g,p\rangle + |e,p + \hbar k\rangle)/\sqrt{2}$, with the excited state gaining a photon recoil $\hbar k$ relative to the ground state part of the wavepacket ($k = 2\pi/\lambda$). A "mirror" π pulse drives an atom from the ground to the excited state, $|g,p\rangle \rightarrow |e,p + \hbar k\rangle$, imparting a photon recoil kick, or vice versa, which causes a stimulated emission of a photon and reduction of momentum. We applied a $\pi/2$-π-$\pi/2$ interferometer sequence with a pulse separation T (Fig. 2). The initial $\pi/2$ pulse separates the two wavepackets because of the difference in their momentum. The π pulse redirects the wavepacket momentum, causing the two components to overlap again at time $2T$, when the final $\pi/2$ pulse induces their interference. Momentum recoil creates different trajectories for the wavepackets that acquire a relative gravitationally induced atomic phase shift during the interferometer,

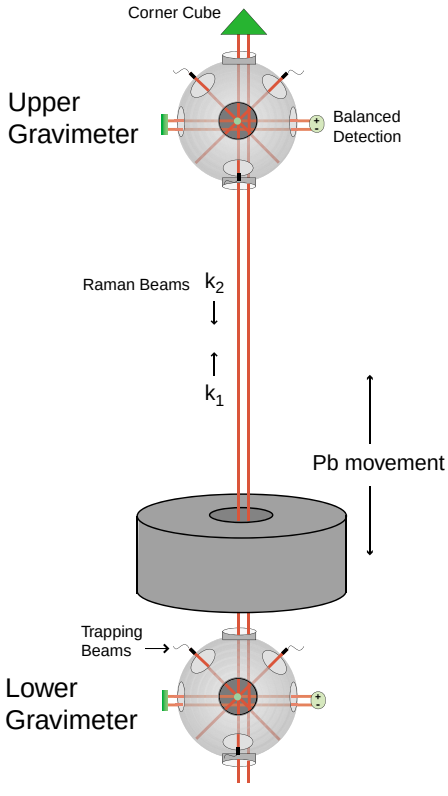

Fig. 1. Schematic of the experiment. The Raman beams propagate along a common vertical axis that contains both atomic ensembles (*20*).

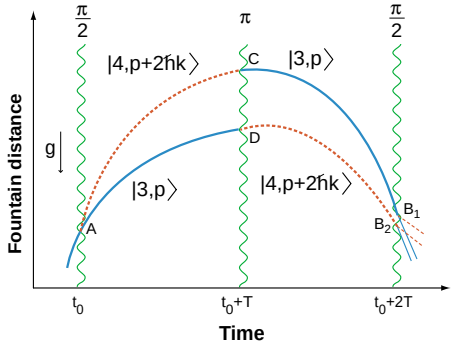

Fig. 2. Recoil space diagram of the atoms through the interferometer showing the separation (exaggerated) of the atomic wavepackets (*20*). A, initial $\pi/2$ pulse; B1, final $\pi/2$ pulse (upper trajectory); B2, final $\pi/2$ pulse (lower trajectory); C, π pulse (upper trajectory); D, π pulse (lower trajectory).

[1]Department of Physics, Stanford University, Stanford, CA 94305–4060, USA. [2]Department of Physics and Astronomy, City University of New York, Hunter College, New York, NY 10021, USA. [3]Department of Physics, Simon Fraser University, Burnaby, British Columbia, V5A 1S6, Canada.

*To whom correspondence should be addressed. E-mail: kasevich@stanford.edu

resulting in a sensitivity to accelerations. The total phase shift, $\Delta\phi_{Tot}$, is the sum of three components: the interaction of the atom with the light pulse, $\Delta\phi_{Laser}$; the quantum propagation phase accrued by each wavepacket over its trajectory, $\Delta\phi_{Path}$; and the wavepacket overlap, $\Delta\phi_{Separation}$ (*17*, *18*).

Operation of the gravity gradiometer has previously been described in detail (*15*, *19*, *20*). The two gravimeters are separated by 1.347 m, sharing a common vertical measurement axis. In each gravimeter chamber, we loaded Cs atoms into a magneto-optical trap (MOT) (*21*). The same trapping lasers used in the MOT then launched the atoms upward on a 12-cm ballistic trajectory. The interferometer pulses drove Doppler-sensitive two-photon optical (λ = 852 nm) Raman transitions (*22*) between the $F = 3$ and $F = 4$ hyperfine ground states. At the end of the interferometer, the probability that atoms will be in the $F = 4$ ground state for each gravimeter follows (*16*):

$$P_{|4\rangle} = \frac{1}{2}[1 - \cos(\phi_0 + \Delta\phi)] \qquad (1)$$

where $\Delta\phi$ contains the gravitationally induced phase shift. Acousto-optic modulators in the Raman path are used to phase scan the fringe by changing ϕ_0. The transition probability is determined by detecting the atoms in both hyperfine states after the interferometer sequence with the use of a balanced, modulation-transfer technique (*23*).

Accelerations of the reference frame of the Raman laser field will result in phase shifts that are indistinguishable from gravitational accelerations by the Equivalence Principle. The gradiometer difference of simultaneous acceleration measurements in the same reference frame allows for rejection of vibrational noise. However, more than $(5 \times 10^{-7})g$ of environmental noise washes out the fringe contrast. We developed a technique to analyze the individual noisy data from the two gravimeters (*24*) that takes advantage of the idea that the two gravimeter signals parametrically describe an ellipse. Common phase noise in the two sinusoids distributes the data points around the ellipse but does not change the ellipticity. The ellipticity is proportional to the gravity-gradient phase difference. We used ellipse-specific fitting routines to extract the differential phase shift between the gravimeters without the need for the actively stabilized reference platform that would otherwise be required for individual fringe fitting.

The Pb source mass consisted of 20 stacked 2.5-cm-thick plates with an outer diameter of 35.3 cm and an inner bore with a diameter of 7.0 cm. The source was suspended between the gravimeters on a type 314 stainless steel platform, with a center bore, attached to an Al support frame. A stepper motor translated the frame vertically between the gravimeters, guided along a similar frame on Teflon pads. Two matched ball-screw jacks permitted high movement accuracy and repeatability, measured at 555 and 31 ppm, respectively.

We made a series of differential measurements of phase shifts induced by the Pb source at two positions, near the top of the lower gravimeter and 27.940 cm higher near the center of the gradiometer. The difference between the signal at the low and high positions provided a high level of rejection against possible systematic phase shifts that do not depend on the Pb position, including alternating-current Stark shifts, tidal field fluctuations, electronic offsets, and the Coriolis force. We periodically reversed the effective Raman propagation vector to gain further immunity to systematic phase offsets (*20*). A single data set typically lasted 7.6 hours.

During signal acquisition, the interferometer signal amplitudes, signal contrast, magnetic fields, laser-diode amplitudes, and room temperature were monitored. The gradient phase shift was observed to be independent of drifts in these parameters to within statistical deviations from a collection of data runs ($<5 \times 10^{-9}$ m/s^2). The phase was sensitive to the Raman lasers coming out of injection lock. This also produced a strong change in the signal amplitude or contrast, which allowed straightforward rejection during analysis.

The filtered data then was fit with the ellipse-specific routine. The output phases were separated into the two propagation phases and the two Pb positions. The phase data was then averaged for each position and propagation direction and combined to yield a mean chop phase difference for the data run. Standard deviations of the fitted subsets determined the phase uncertainty. A typical series of analyzed phase data is shown in Fig. 3. The modulation of the phase is clearly visible. The inset shows a typical 16-point fringe scan.

To determine a value for G from our differential chopped phase measurement, we modeled the expected signal from the Pb source potential. The model required accurate knowledge of the atomic trajectories in the two gravimeters, their respective distances to the Pb source distribution, and the Pb source characteristics (including Pb density and geometry). Given that the calculated total phase shift (*20*) exhibits a linear dependence on the initial trajectory position and velocity over the experimentally relevant range of initial conditions, the atom ensemble–averaged total phase shift is simply determined by the phase shift associated with the mean (measured) ensemble position and velocity. The ensemble position was determined with the use of resonance fluorescence and the velocity by time of flight (*20*).

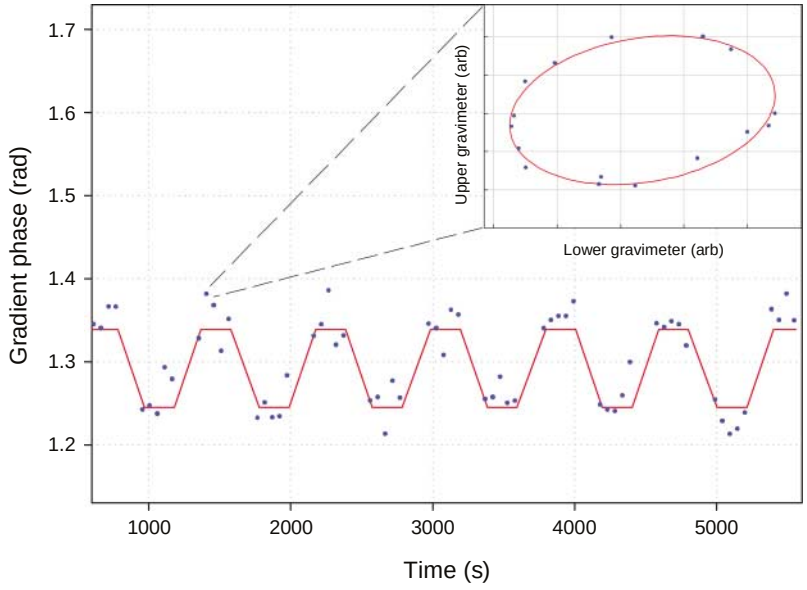

Fig. 3. A typical data sequence showing a modulation of the gradiometer phase output as the Pb source mass is displaced 27.940 cm from the top of the lower chamber. Data points are the fit phase of 16-point fringe scans. The single scan scatter was typically 35 mrad. The gravitational force from the Pb caused a differential acceleration of about $(\sim 30 \times 10^{-9})g$ between the two interferometer signals. Solid trace shows the theoretical values. (Inset) A parametric plot of a typical 16-point scan with the ellipse-specific fit. arb, arbitrary units.

Table 1. Uncertainty limits.

Systematic	$\delta G/G$
Initial atom velocity	1.88×10^{-3}
Initial atom position	1.85×10^{-3}
Pb magnetic field gradients	1.00×10^{-3}
Rotations	0.98×10^{-3}
Source positioning	0.82×10^{-3}
Source mass density	0.36×10^{-3}
Source mass dimensions	0.34×10^{-3}
Gravimeter Separation	0.19×10^{-3}
Source mass density inhomogeneity	0.16×10^{-3}
Total	3.15×10^{-3}

Given the initial velocity and position, we determined the atom trajectories and then numerically solved for the total phase shift $\Delta\phi_{Tot} = \Delta\phi_{Laser} + \Delta\phi_{Path} + \Delta\phi_{Separation}$ using the exact potential of the source mass distribution (including the dominant contribution from the Pb as well as contributions from the stainless steel plate and support rods) and the second-order Taylor expansion of the Earth potential (*17*, *18*). Because the source mass potential depends linearly on G, the resulting total phase shift also depends on G. Thus, comparison of the calculated and observed shifts can be used to measure G. Evaluation of the term $\Delta\phi_{Path}$ involves an integral over the classical action for the calculated atomic trajectories. The term $\Delta\phi_{Separation}$ arises from the spatial separation of the two interfering wavepackets following the final $\pi/2$ pulse (this term is zero for uniform gravitational acceleration) and is obtained directly from the atomic trajectories. Finally, the term $\Delta\phi_{Laser}$ results from the light-pulse interactions and is determined by the phases of the laser fields evaluated at the semiclassical (mean) positions of the wavepackets during each of the laser-atom interactions. This term is also obtained directly from the atomic trajectories.

The semiclassical path-integral formalism that we used to extract G contains several approximations. An exact calculation would involve integration of Schödinger's equation for a wavepacket subject to the laser-pulse sequence and the gravitational potential of the source mass and Earth. Such a calculation is computationally intractable. We estimated that any deviation from the path-integral formalism resulting from the Gaussian wavepackets and nonquadratic potential terms from the Pb source was negligible (*20*). Terms associated with the Earth rotation were determined to produce negligible phase shifts in the differential phase shift.

Combining the above model with the experimentally measured phase shift, we determined a value of $G = 6.696 \times 10^{-11} \pm 0.037 \times 10^{-11}$ $m^3/(kg \cdot s^2)$ for data run 1. The integration period lasted for 54 data sets. The Pb source mass gravitational phase shifts from the two run cycles are represented in Fig. 4. After a study of potential systematic sources of error on the interferometer phase shift, we performed a repeat measurement. In the latter study we placed the Pb mass 0.635 cm higher than for data run 1, maintaining a 27.940-cm displacement cycle. Furthermore, we reordered the individual Pb disks comprising the source mass. We obtained a value of $G = 6.691 \times 10^{-11} \pm 0.041 \times 10^{-11}$ $m^3/(kg \cdot s^2)$ in the second integration period, lasting 39 data sets. We performed analysis tests similar to those used on the first data run, with the results from runs 1 and 2 agreeing to within statistics. Combining the two measurements results in a statistical value of $G = 6.693 \times 10^{-11} \pm 0.027 \times 10^{-11}$ $m^3/(kg \cdot s^2)$. The bottom plot of Fig. 4 shows our data and its agreement with CODATA. Several G measurements mentioned in the text are listed for comparison.

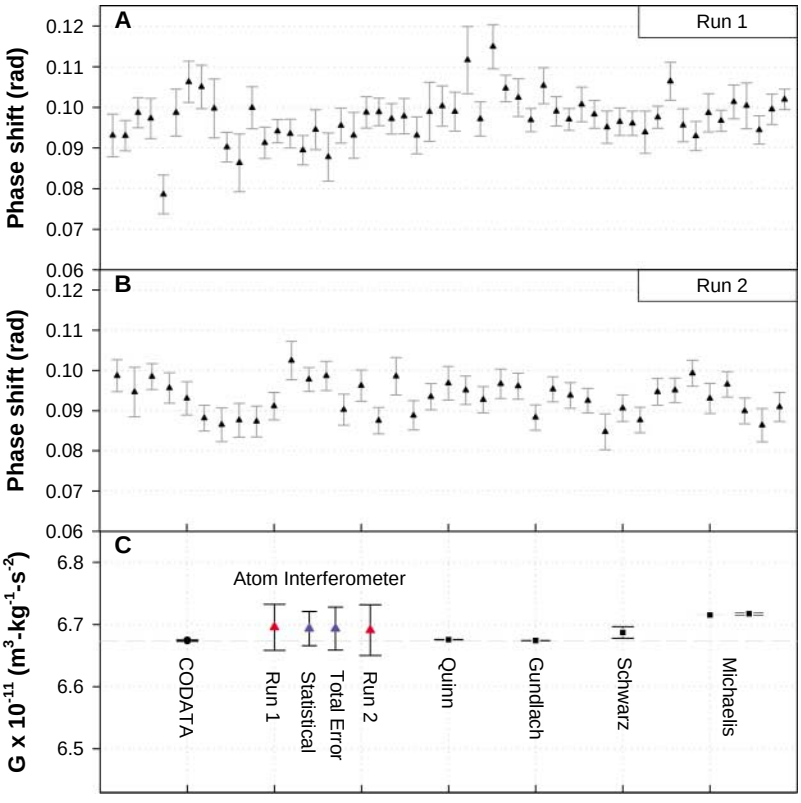

Fig. 4. Data used in the determination of G. (**A**) A data sequence consisting of 51 data sets. Analysis of the phase shifts resulted in a value for $G = 6.696 \times 10^{-11} \pm 0.037 \times 10^{-11}$ $m^3/(kg \cdot s^2)$. (**B**) A second measurement of G with a different initial vertical position of the source mass and a redistribution of the individual discs comprising the Pb stack. The same analysis as the first measurement gave a value of $G = 6.691 \times 10^{-11} \pm 0.041 \times 10^{-11}$ $m^3/(kg \cdot s^2)$. (**C**) Combined results of our measurements agree within statistical uncertainties of each other and of the CODATA value, resulting in $G = 6.693 \times 10^{-11} \pm 0.027 \times 10^{-11}$ $m^3/(kg \cdot s^2)$ (statistical error) and $6.693 \pm 0.021 \times 10^{-11}$ $m^3/(kg \cdot s^2)$ (systematic error). Also shown (left to right) are values reported in Quinn *et al.* (*10*), Gundlach and Merkowitz (*9*), Schwarz *et al.* (*4*), and Michaelis *et al.* (*11*). Error bars show means ± SD.

Knowledge of how the accuracy of our measurement is affected by environmental and device parameters is crucial for a future precision measurement of G with our technique. The results of these tests are summarized in Table 1. Systematic uncertainties limited our experiment to an accuracy of 3 ppt. The dominant systematics were the knowledge of the atom initial position and velocity.

The source mass was specified as 99.99% pure Pb. We characterized the dimensions of the disks and steel plate to 1 ppt with precision calipers and the mass to 40 ppm using a calibrated scale. A volume displacement technique was used to test the density homogeneity of small samples cut from a number of separate Pb disks not used in the G measurement. Density variation was determined to be 260 ppm. Estimating an upper bound of less than 1% radial and longitudinal density inhomogeneities contributes a 0.02% systematic in determining G.

The small residual magnetization of the steel plate used to hold the Pb caused spurious phase shifts through two mechanisms. These shifts were studied by applying additional, much stronger, magnetic sources to the platform. We characterized magnetic fields with the use of Doppler-free Raman spectroscopy of magnetically sensitive hyperfine transitions (an in situ method) and also with the use of a fluxgate magnetometer. The first shift results from second-order Zeeman shifts associated with magnetic field gradients present during the fountain sequence. Propagation reversal of the Raman beams suppresses this shift, but it cannot be completely eliminated because the reversed interferometer paths differ slightly from the nonreversed paths. The second shift results from a Coriolis phase shift that originated in an additional transverse velocity component induced by the presence of a residual magnetic field during the launch. On the basis of the measured residual magnetization of the plate, we estimated that each of these shifts contributed systematic uncertainties of 0.1%.

The gravitational potential of the Pb cylindrical geometry afforded an insensitivity to radial displacements at the 10-ppm level over 5 mm of radial translation. However, we initially found a 5-mrad/mm dependence on the position of the Pb in the plane perpendicular to the interferometer axis. In situ measurements of the magnetic field

at various source mass positions revealed source mass–dependent eddy magnetic fields induced by the switching of the MOT coils. After we implemented a controlled decrease of the field (rather than a sudden switch), we no longer saw a statistically significant dependence on the transverse position of the source for deviations as large as 1 cm.

We individually offset other parameters to values beyond accepted operating characteristics of the gradiometer, often to the point at which the interferometer fringe contrast decreased to below ~10% (typical contrast was 25%). These variables included Doppler sensitive π- and π/2-pulse lengths, position of atoms in the detection probe beam, detection efficiency, launch angle, off-resonant Raman light, initial $m_f \neq 0$ population (where m_f indicates the Zeeman sublevel), scattering from the background Cs vapor, Raman light intensity, and Raman wavefront quality. Experiments involved the measurement of the Pb-induced phase shift for large offsets in each of the above parameters. At these large offsets, we observed no systematic dependence on the mass displacement signal. From these measurements, we inferred that small drifts of these parameters in time do not contribute systematic offsets in our determination of G.

We looked for systematic effects in our analysis by varying the analysis procedures and parameters. For example, we varied the contrast and outlying phase thresholds used to filter wild points. In this case, we found that for all sets in runs 1 and 2, the inferred values for G agreed to within the statistics. We also studied the effect of the scaling parameters used within the normalized detection scheme to search for possible bias (*25*). Improper normalization resulted in values for G within statistics, whereas the statistical uncertainties increased for large deviations from optimal parameters.

Our demonstrated proof-of-principle measurement of the Newtonian constant of gravity based on atom interferometric measurement of gravity-induced phase shifts presents a technique for the measurement of G not subject to the known and hidden systematics of previous measurements. Since the completion of this work, the experiment of Tino *et al.* (*26*) has begun construction of an atom interferometer apparatus with the goal of increasing the sensitivity and decreasing the systematics to perform a measurement of $\delta G/G = 10^{-4}$.

References and Notes

1. P. J. Mohr, B. N. Taylor, *Rev. Mod. Phys.* **77**, 1 (2005).
2. U. Kleinevoß, H. Meyer, A. Schumacher, S. Hartmann, *Meas. Sci. Technol.* **10**, 492 (1999).
3. F. Nolting, J. Schurr, S. Schlamminger, W. Kündig, *Meas. Sci. Technol.* **10**, 487 (1999).
4. J. P. Schwarz, D. S. Robertson, T. M. Niebauer, J. E. Faller, *Science* **282**, 2230 (1998).
5. C. V. Boys, *Philos. Trans. R. Soc.* **186**, 1 (1895).
6. P. R. Heyl, P. Chrzanowski, *J. Res. Natl. Bur. Std. U.S.* **29**, 1 (1942).
7. G. T. Gillies, *Rep. Prog. Phys.* **60**, 151 (1997).
8. P. J. Mohr, B. N. Taylor, *Rev. Mod. Phys.* **72**, 351 (2000).
9. J. H. Gundlach, S. M. Merkowitz, *Phys. Rev. Lett.* **85**, 2869 (2000).
10. T. J. Quinn, C. C. Speake, S. J. Richman, R. S. Davis, A. Picard, *Phys. Rev. Lett.* **87**, 111101 (2001).
11. W. Michaelis, H. Haars, R. Augustin, *Metrologia* **32**, 267 (1995).
12. K. Kuroda, *Meas. Sci. Technol.* **10**, 435 (1999).
13. W. Michaelis, J. Melcher, H. Haars, *Metrologia* **41**, L29 (2004).
14. A. Peters, K. Y. Chung, S. Chu, *Metrologia* **38**, 25 (2001).
15. J. M. McGuirk, G. T. Foster, J. B. Fixler, M. J. Snadden, M. A. Kasevich, *Phys. Rev. A.* **65**, 033608 (2002).
16. P. Berman, Ed., *Atom Interferometry* (Academic Press, New York, 1996).
17. K. Bongs, R. Launay, M. A. Kasevich, *Appl. Phys. B* **85**, 602 (2006).
18. P. Storey, C. Cohen-Tannoudji, *J. Phys. II* **4**, 1999 (1994).
19. M. J. Snadden, J. M. McGuirk, P. Bouyer, K. G. Haritos, M. A. Kasevich, *Phys. Rev. Lett.* **81**, 971 (1998).
20. Materials and methods are available as supporting material on *Science* Online.
21. E. L. Raab, M. Prentiss, A. Cable, S. Chu, D. E. Pritchard, *Phys. Rev. Lett.* **59**, 2631 (1987).
22. M. Kasevich *et al.*, *Phys. Rev. Lett.* **66**, 2297 (1991).
23. J. M. McGuirk, G. T. Foster, J. B. Fixler, M. A. Kasevich, *Opt. Lett.* **26**, 364 (2001).
24. G. T. Foster, J. B. Fixler, J. M. McGuirk, M. A. Kasevich, *Opt. Lett.* **27**, 951 (2002).
25. Detection-laser powers were periodically adjusted to optimize the detected atom number and signal-to-noise ratio, which results in a slight change of the normalization coefficients, $\alpha_{L,U}$. The normalized $|4,0\rangle$ population is $S_1/(S_1 - \alpha_{L,U}S_2)$, where $S_{1,2}$ is proportional to the $|4,0\rangle$ and $|4,0\rangle - |3,0\rangle$ signal, respectively.
26. A. Bertoldi *et al.*, *Eur. Phys. J. D* **40**, 271 (2006).
27. This work was supported by grants from the ONR and NASA.

Supporting Online Material

www.sciencemag.org/cgi/content/full/315/5808/74/DC1
Materials and Methods
References

22 September 2006; accepted 22 November 2006
10.1126/science.1135459

Conductance-Controlled Point Functionalization of Single-Walled Carbon Nanotubes

Brett R. Goldsmith,[1] John G. Coroneus,[2] Vaikunth R. Khalap,[1] Alexander A. Kane,[1] Gregory A. Weiss,[2,3] Philip G. Collins[1]*

We used covalent attachments to single-walled carbon nanotubes (SWNTs) to fabricate single-molecule electronic devices. The technique does not rely on submicrometer lithography or precision mechanical manipulation, but instead uses circuit conductance to monitor and control covalent attachment to an electrically connected SWNT. Discrete changes in the circuit conductance revealed chemical processes happening in real time and allowed the SWNT sidewalls to be deterministically broken, reformed, and conjugated to target species. By controlling the chemistry through electronically controlled electrochemical potentials, we were able to achieve single chemical attachments. We routinely functionalized pristine, defect-free SWNTs at one, two, or more sites and demonstrated three-terminal devices in which a single attachment controls the electronic response.

Covalently linking a single molecule of interest between two electrical conductors enables the electrical interrogation of that molecule as it dynamically interacts with the surrounding environment. In practice, however, working single-molecule devices remain exceedingly difficult to fabricate (*1*). Successes based on very small electrode gaps fabricated lithographically (*2*), electrically (*3*, *4*), or by scanning probe techniques (*5*, *6*) generally suffer from low fabrication throughput; electrical, mechanical, and chemical instabilities; poorly defined bonding to the molecule of interest; and, sometimes, inconclusive proof that only a single molecule is addressed.

Single-walled carbon nanotubes (SWNTs) have several favorable characteristics for building high-quality, single-molecule devices. Electrically, they are high-conductivity, one-dimensional (1D) conductors that can deliver signals to and from attached molecules. Chemically, SWNTs have long, inert sidewalls but reactive ends to which the tools of organic chemistry can covalently attach a wide variety of species (*7*). Geometrically, SWNTs' small profile maximizes access to the target molecule by reagents, optical probes, or electrostatic fields. Many strategies for building functioning, nanometer-scale circuits have focused on complex manipulation or high-resolution lithographies (*8*–*11*). Guo *et al.*, for example, have beautifully demonstrated single-molecule junctions in broken SWNTs by combining <10-nm lithography with plasma etching (*11*).

Here, we describe an alternative technique that does not require high-resolution lithography and is effective for molecules of any size. The general scheme is to fabricate circuits using individual SWNTs and then use the SWNT conductance G as a real-time indicator of SWNT chemical modification. With the use of electrochemically driven reactions, the introduction of functional groups can be electronically controlled and monitored with microsecond tempo-

[1]Department of Physics and Astronomy, University of California, Irvine, CA 92697, USA. [2]Department of Molecular Biology and Biochemistry, University of California, Irvine, CA 92697, USA. [3]Department of Chemistry, University of California, Irvine, CA 92697, USA.

*To whom correspondence should be addressed. E-mail: collinsp@uci.edu